Salt Solubility and Deposition in High Temperature and Pressure Aqueous Solutions

Marc Hodes and Peter Griffith
Mechanical Engineering Dept., Massachusetts Institute of Technology, Cambridge, MA 02139

Kenneth A. Smith
Chemical Engineering Dept., Massachusetts Institute of Technology, Cambridge, MA 02139

Wilbur S. Hurst and Walter J. Bowers, Jr.
Chemical Science and Technology Laboratory, Process Measurements Division, National Institute of Standards and Technology, Gaithersburg, MD 20899

Kentaro Sako
Analysis and Simulations Center, Asahi Kasei Corporation, Shizuoka 416-8501, Japan

DOI 10.1002/aic.10238
Published online in Wiley InterScience (www.interscience.wiley.com).

Solubility and deposition rate experiments were performed in aqueous sodium sulfate and potassium sulfate solutions at elevated temperatures and pressures typical of the supercritical water oxidation (SCWO) process. The test cell was a six-port chamber in the form of a modified 1.91 cm (3/4 in.) diameter Swagelok cross with an internally heated cylinder (hot finger) mounted in its center. Solubilities were acquired by maintaining the surface temperature of the hot finger about 10°C above the gradually increasing bulk temperature of the solution flowing by it until salt precipitated on the hot finger. Solubility temperatures for sodium sulfate and potassium sulfate in water were measured for salt concentrations of up to 10% mass fraction. In the deposition rate experiments, the solution flowing past the hot finger was preheated to a temperature close to the solubility temperature and the salt layer–solution interface formed on the hot finger was maintained slightly above the solubility temperature to drive deposition. Deposition rates from SCWO streams containing up to 8% mass fraction salt were obtained by measuring the mass of the salt deposited on the hot finger after each (6 to 12 min) run. Solubility data are compared to those from other studies and a simple deposition rate model is developed and compared with the deposition rate data. Natural convection dominated transport and the system pressure was 25 MPa at all conditions. © 2004 American Institute of Chemical Engineers *AIChE J,* 50: 2038–2049, 2004

Keywords: deposition rate, supercritical water oxidation (SCWO), hot finger, natural convection, solubility

Introduction

Toxic organic wastes and "mixed wastes," composed of toxic organic compounds and radioactive elements, are a major environmental management problem. Supercritical water oxidation (SCWO), defined as oxidation in water at temperatures and pressures exceeding the critical temperature (371°C) and critical pressure (22.1 MPa) of pure water, is an effective technology for treatment of these wastes (Shaw et al., 1991; Tester et al., 1993). It destroys their organic constituents and, when necessary, concentrates their radioactive ingredients in forms suited to safe disposal. For widespread commercializa-

Correspondence concerning this article should be addressed to M. Hodes at this current address: Bell Laboratories, Rm. 1C-462, 600 Mountain Ave., Murray Hill, NJ 07974; e-mail: Hodes@lucent.com.

tion of SCWO to be realized, corrosion and scale buildup (fouling), caused by the production of "sticky" salts, must be controlled. Corrosion of SCWO reactor materials caused by acidic solutions that result from the oxidation of organic compounds containing heteroatoms such as S, Cl, or P is often minimized by injecting neutralizing bases into the reactor. The salts formed upon neutralization (sulfates, chlorides, phosphates, etc.) have low solubility in supercritical water (SCW) and, consequently, precipitate as solid phases. (Salts may also be present in the waste stream itself.) Because the salts tend to be "sticky," they can form agglomerates and coat internal surfaces, thereby leading to plugging and inhibition of heat transfer. When a reactor or transport line becomes plugged, it becomes necessary to remove the plug by flushing it out with cold water (or cold solution), by mechanical means, or by chemical means (acid washes). Often, this results in substantial and costly downtime in the SCWO process. Hodes et al. (2003a) further discuss the scale control problem and review pertinent aspects of phase behavior, heat transfer, and mass transfer in an SCWO environment. Reactor designs and specific operating techniques for the control of scale buildup during SCWO are reviewed by Marrone et al. (2004).

Solubility and deposition rate measurements in aqueous sodium sulfate and potassium sulfate solutions at the elevated temperatures and pressures found in SCWO are presented in this study. Rogak and Teshima (1999) examined deposition of salt in turbulent flows through a tubular reactor at SCWO conditions, but other investigators have not measured deposition rates under tightly controlled conditions. The aqueous salt systems and photographs of the salts deposited on a hot finger are discussed next. Then the experimental apparatus, procedure, and data are presented. Finally, the solubility data collected are compared to those in the literature and a simple model to predict deposition rate is developed and applied to the experimental conditions.

The temperature–composition diagram for the aqueous sodium sulfate system at 25 MPa is shown in Figure 1 and that for the aqueous potassium sulfate system is qualitatively similar. The solubility curve separates a single-phase–fluid region from a two-phase (fluid and solid salt) region. Experimental determinations of solubilities were acquired by maintaining the surface temperature of a hot finger approximately 10°C above the bulk temperature of the solution flowing by it. The hot finger surface temperature at which precipitation first occurs is the solubility temperature. In the deposition rate experiments, the aqueous salt solution flowing pass the hot finger was preheated to a temperature close to that at which precipitation begins and the salt layer–solution interface (SLSI) formed on the hot finger was maintained a few degrees centigrade above this precipitation temperature. This yielded about a 2% mass fraction driving force for deposition at the SLSI. Laminar natural convection dominated transport at all conditions in this study (Hodes, 1998). The weak cross flow of solution pass the hot finger served only to maintain the temperature and concentration in the bulk solution as close to constant as possible.

Photographs of a 5.08 mm (0.200 in.) OD hot finger before and after it was inserted into the cross flow of an aqueous sodium sulfate solution of mass fraction 4% flowing (laminarly) at 10.47 g/min for about 15 min are shown in Figure 2. (Initial bulk solution and hot finger surface conditions are shown in Figure 1.) The cross flow is directed vertically upward (that is, in the direction opposite to that of the gravity vector) as indicated. Figure 3 shows a photograph of the hot finger after it was inserted into the cross flow of an aqueous potassium sulfate solution of mass fraction 4% flowing (laminarly) at 10.39 g/min for about 10 min. The structure of the potassium sulfate formed on the hot finger was clearly dendritic, whereas obvious dendrites were not observed when sodium sulfate was deposited. The thicknesses of the salt layers formed on the hot finger were on the order of the radius of the hot finger after only 10 min of deposition, illustrating the severity of the scale buildup problem that can occur during SCWO. It is noted that the potassium sulfate was easily removed from the hot finger with one's fingers. The sodium sulfate, however, generally had to be removed by mechanical means unless it was loosened with tap water.

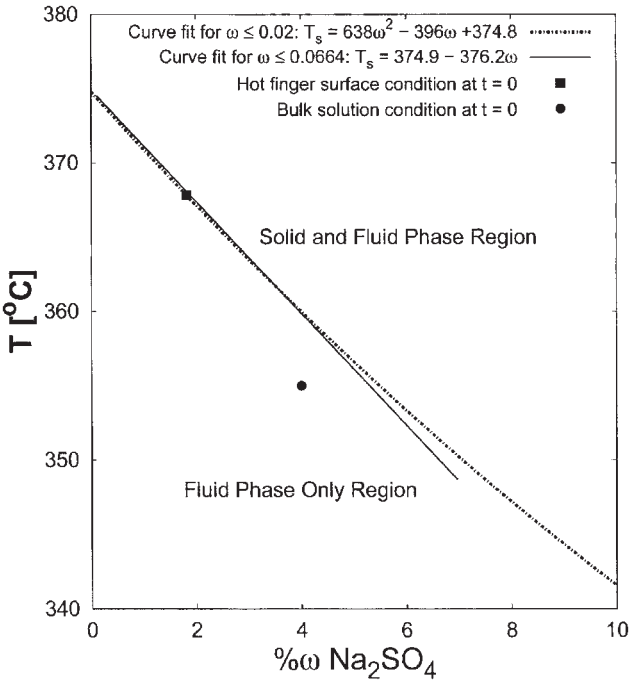

Figure 1. Temperature–composition diagram for the Na_2SO_4–H_2O system at 25 MPa based on linear and 2nd-order curve fits to existing data compiled by Hodes et al. (2004).

Initial bulk solution and hot finger surface conditions for the deposition experiments in which the mass fraction of Na_2SO_4 in the (inlet) solution was 4% are indicated.

Experiments

Apparatus

The experimental apparatus is described by Hurst et al. (2002) and shown in Figure 4. The test cell is a six-port chamber with an internal volume of 17 mL. One port was used to mount a hot finger into the center of the chamber and the others provided fluid cross flow, windows for illumination and visual observation, and a thermocouple to measure bulk solution temperature.

The hot finger is shown in Figure 5. The Hastelloy C276–sleeved copper portion of it protrudes into the test cell and serves as the deposition surface along with a small part of the

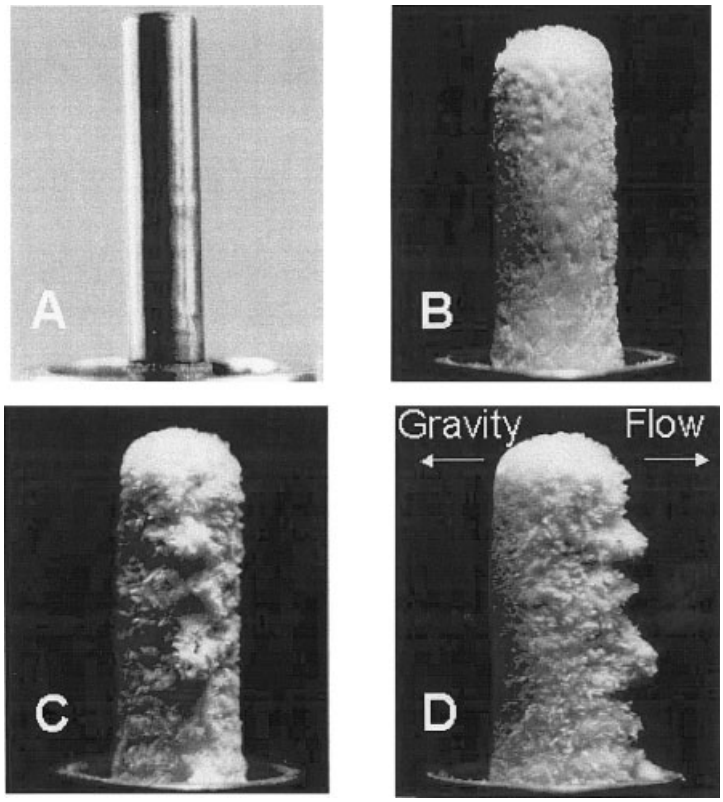

Figure 2. Photograph of the 5.08 mm OD hot finger before insertion into the cross flow of an aqueous sodium sulfate solution with mass fraction 4% and upstream, downstream, and side views of it after about 15 min of exposure.

Flow direction and gravity vector are shown in side view. (T_B = 356°C, pressure = 25 MPa, $\dot{m}_{soln}$ = 10.47 g/min).

Inconel 625 base. The portion of the hot finger on which salt deposits is 27.58 mm (1.086 in.) long and its diameter is 5.08 mm (0.200 in.), except for the 3.43 mm (0.135 in.) closest to the base where it slightly increases. In all the experiments, 10.6 W of (constant) power was supplied to the hot finger by a cartridge heater inside it. Two hot fingers were fabricated. One of them was instrumented with five 0.25 mm (10 mils) diameter, Incoloy-sheathed, type K thermocouples to measure surface temperatures at the locations shown in Figure 5. Thermocouple F4 is located at the forward stagnation point on the upstream side of the hot finger exactly in the middle of the protruding portion. Thermocouples F3 and F2 are located 90 and 180° azimuthally downstream of thermocouple F4, respectively. Thermocouples F1 and F5 are located 2.13 and 0.64 cm (0.84 and 0.25 in.) away from the tip of the hot finger, respectively, at the same azimuthal location as thermocouple F3. Each thermocouple enters the test cell through a hole in the base of the hot finger and runs axially along the protruding portion of the hot finger to the position indicated in Figure 5. Silver solder anchored the thermocouples along the hot finger and secured their junctions to it. When deposition rate data are collected, the hot finger must be installed and removed for each run. Because the 0.25 mm (10 mils) diameter thermocouples are extremely fragile, a second (identical) hot finger without thermocouples was used in the deposition rate experiments.

The entire test cell is housed inside an insulated aluminum block that is maintained near the temperature of the fluid at the preheater outlet using embedded cartridge heaters. The system is connected to a high pressure compressed nitrogen line and a bypass line is available to flush out the aqueous salt solution after a deposition run as described below. Heat transfer experiments were performed with pure water to validate the flow system. The measured hot finger surface-to-bulk temperature differences were always within the uncertainties of those predicted by standard convection heat-transfer correlations (Hodes, 1998).

Procedure

Solubility Experiments. Before each solubility experiment, low-temperature (≤100°C) distilled water is circulated through the flow system to dissolve and remove any salt that may be present. [The flow rates of water/solution in all experiments were 10 mL/min at room temperature (about 20°C) and pressure (0.1 MPa).] Next, the temperature of the bulk solution in the cell is gradually increased to 250°C. Then the pump is drained and refilled with aqueous salt solution and all pure water is flushed out of the system. At this point, 10.6 W of power are supplied to the hot finger to produce about a 10°C temperature difference between its surface and the bulk fluid. Then the temperature setpoints of the controllers for the preheater and the aluminum block housing the test cell are gradually stepped upward until the surface temperature of the hot finger surface is about 15°C below the salt precipitation tem-

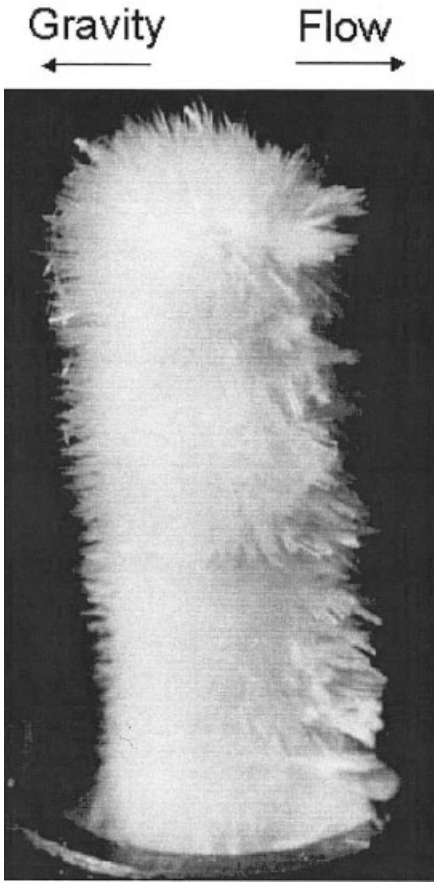

Figure 3. Photograph of the 5.08 mm OD hot finger after insertion into the cross flow of an aqueous potassium sulfate solution with mass fraction 4% for about 10 min.

Flow is from left to right and the gravity vector points from right to left. (T_B = 373°C, pressure = 25 MPa, $\dot{m}$ = 10.39 g/min).

perature. Next, the controller set points are stepped upward at the rate of about 1°C/15 min until salt precipitates on the hot finger. Each 1°C increase in the setpoint temperatures increases the bulk fluid and the hot finger surface temperatures by about 1°C, until precipitation begins. Once a scale layer forms on the hot finger, however, a 1°C increase in bulk fluid temperature causes its surface temperature to increase by about 5°C or more in a 15-min time period. During the solubility experiments, the temperatures measured at the five locations on the hot finger surface were within 3°C of one another until precipitation. Once the scale layer formed, they were consistent to within 4°C. The uncertainty associated with each thermocouple reading is ±3.5°C (see below); therefore, the measured axial and azimuthal variations are of limited significance and the mean surface temperature of the hot finger (based on the five thermocouples) at which precipitation begins is assumed to equal the solubility temperature. Visual observation of nucleation on the hot finger and/or a large increase in its surface temperature for a 1°C increase in bulk fluid temperature indicated the onset of precipitation. In most, but not all, runs nucleation was visually observed before the temperature difference between the hot finger surface and bulk fluid sharply increased. The solubility temperature of the salt at the concentration of interest lies between the highest steady-state temperature of the hot finger surface before precipitation and a temperature about 1°C higher. Thus it is assumed to equal the highest steady-state temperature on the hot finger surface plus 0.5°C. (In runs F and H, the controller set points were increased at the rate of about 2°C/15 min. Thus, the solubility temperature at the concentration of interest is assumed to be the highest hot finger surface temperature measured before deposition plus 1.0°C. Thermocouple F5 did not work in runs L and O.)

If homogeneous nucleation were to occur in the boundary layer, the concentration of salt at the hot finger surface (that is, where solubility temperature is measured) would be unknown. Therefore, the method used to collect solubility data in this study is valid only if the nucleation mechanism when salt begins to deposit is exclusively heterogeneous nucleation on the surface of the hot finger. The nucleation model developed by Smith et al. (2002) predicts that this is always the case. Moreover, visual observations during the experiments yielded no evidence of homogeneous nucleation.

Deposition Experiments. The procedure for the deposition experiments follows that for the solubility experiments until aqueous salt solution flows through the system at 250°C. Then with the bypass line closed (valve D in Figure 4 closed), the controller set points are gradually stepped upward until the bulk temperature of the aqueous salt solution in the cell stabilizes at the desired value. Next, 10.6 W of power are supplied to the hot finger at a time designated as $t = 0$. The surface temperature of the hot finger increases by about 10°C such that it exceeds the salt solubility temperature in the bulk solution and deposition begins. A more detailed explanation of the transient dynamics of the deposition experiments is given by Hodes et al. (2003b). Throughout a run, deposition is visually observed through one of the sapphire windows on the cell using a telescope or CCD camera.

After each run, high pressure nitrogen is used to purge the system of salt solution. This requires about 1.5 min; therefore, purging is started 1.5 min before the desired run time has elapsed. First, power to the preheater before the test cell cell is cut off. Then the pump is turned off and valve A is closed to isolate solution upstream of it. Next, valve B is opened and nitrogen flows into a (concentric) capillary tube inside the cell exit line. This pushes the solution in the exit line through valve C, the effluent heat exchanger, and then out the back pressure regulator. The time at which these lines are free of solution is determined by monitoring the system effluent. At this time, bypass valve D is opened and then valve C is closed. After a few seconds, a nitrogen–solution interface slowly clears the hot finger, which is recorded as the end of the run. Once the effluent is all nitrogen again, valve C is reopened and the nitrogen is pumped through the entire system for at least 30 min to be sure it is completely free of solution and that water vapor does not condense on the deposited salt.

After the cell cools down, the hot finger is carefully removed from the cell with the salt intact and weighed on a balance. Then the salt deposited on the hot finger is loosened with tap water and removed. Once dry, the hot finger is weighed again and subtraction yields the mass of salt deposited on the hot finger. Scraping the salt (sodium sulfate or potassium sulfate) off the hot finger with a dry instrument and exposing it to a desiccant under vacuum for a 3 week period produced no

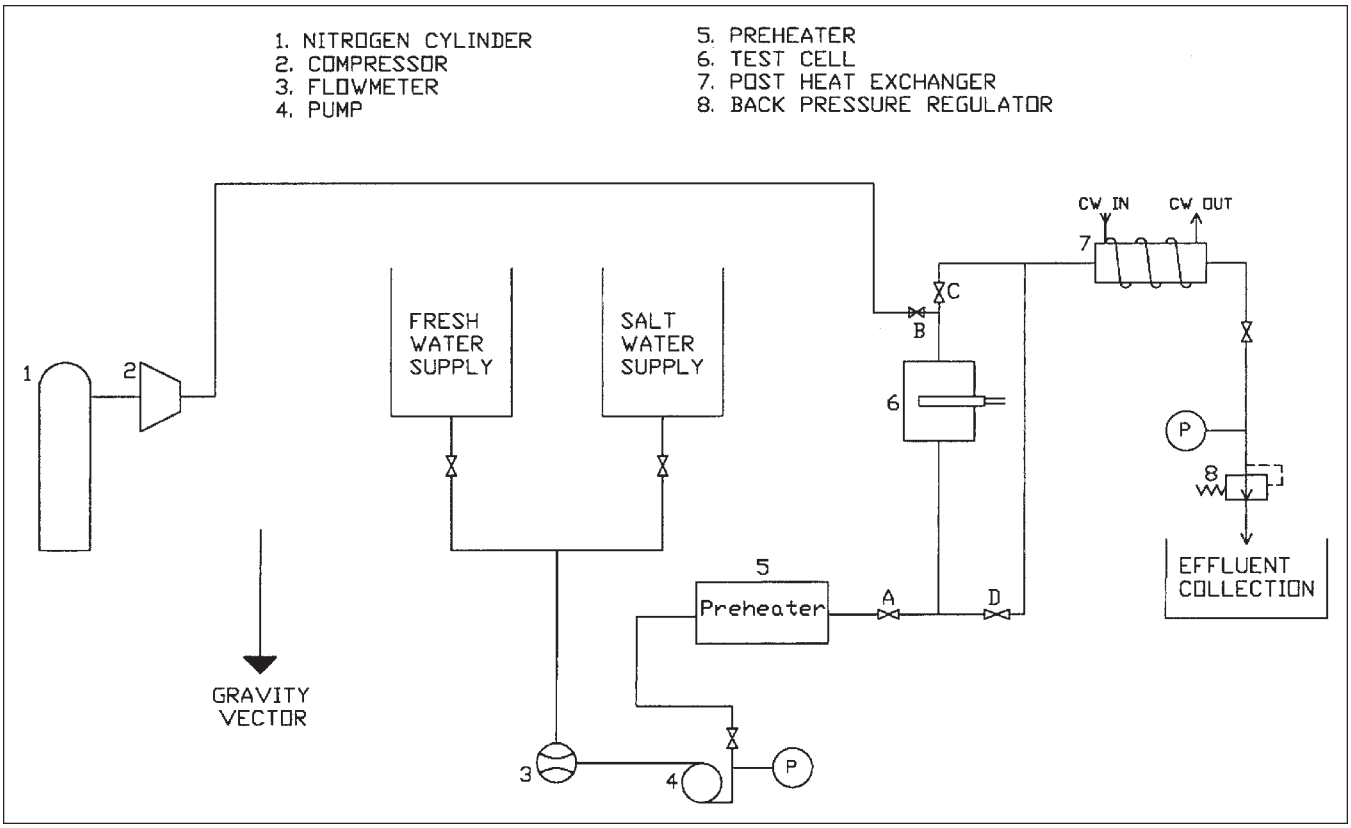

Figure 4. The apparatus.

measurable change in its mass. Therefore, the salt on the hot finger when it is removed from the cell is entirely free of water. Between experiments, the hot finger is handled only with sanitary gloves and the surface of the protruding part is cleaned sequentially with soapy water, isopropanol, and acetone. Then the hot finger is immersed in boiling tap water for a few minutes to dissolve any salt that may be left near its ferrules.

Experimental Data

Uncertainties

Type K commercial-grade thermocouples were used for all temperature measurements. Their calibration tolerance is ±3.00°C at temperatures up to 400°C, according to ASTM Standard E320-87 (ASTM, 1993). The expanded uncertainty for a coverage factor of two, attributed to calibration and instrumentation error in all temperatures reported, is ±3.2°C. The precision of the temperature measurements has been estimated to be ±0.5°C. The mass flow rate of fluid delivered by the ISCO pump is within ±0.05 mL/min of that selected and constant to within ±0.01 mL/min during operation according to ISCO literature. (Certain commercial equipment and instruments are identified herein to adequately specify the experimental procedure. In no case does such identification imply recommendation or endorsement by the National Institute of Standards and Technology, nor does it imply that the equipment identified is necessarily the best available for the purpose.) The Sensotec Model GM pressure transducers and Sensotec Model LM signal conditioners that accompany them are factory calibrated to ±0.15 MPa. The standard uncertainty of the power dissipated by the cartridge heater inside of the hot finger was ±4.25% (0.45 W), based on measured fluctuations in the voltage supplied to it, voltage measurement uncertainties, and the measured resistance of the heater as a function of temperature.

Based on visual observations of the hot finger during the procedure by which the system is purged of solution (blow-down), it is estimated that from 5 to 20% of the salt deposited on it is eroded away. Formation of the bumps shown in Figure 2 and of the pronounced dendrites shown in Figure 3 is visually observed during deposition and is not a consequence of erosion during blow-down. Moreover, there is no evidence of erosion before blow-down. The time at which the nitrogen interface clears the hot finger during the blow-down procedure (which marks the end of a run) is measured to within 3 s by using a stopwatch. The mass of salt deposited on the hot finger is measured using an Ohaus Model AP210S balance, accurate to within ±0.02 g.

The thermal capacitance of the entire hot finger is small and it is estimated that less than 3% of the total energy supplied to it during the deposition experiments is consumed in heating it (Hodes, 1998). A 0.32 cm (1/8 in.) OD, Incoloy-sheathed, type K thermocouple was used to measure the bulk fluid temperature in the test cell. The length-to-diameter ratio of the portion of the thermocouple exposed to fluid in the cell is only 0.8. Nonetheless, the bulk temperature measurement has been estimated to have a ±4.2°C expanded uncertainty for a coverage factor of two, inclusive of all sources of error (Hodes, 1998). The expanded uncertainty for a coverage factor of two for the

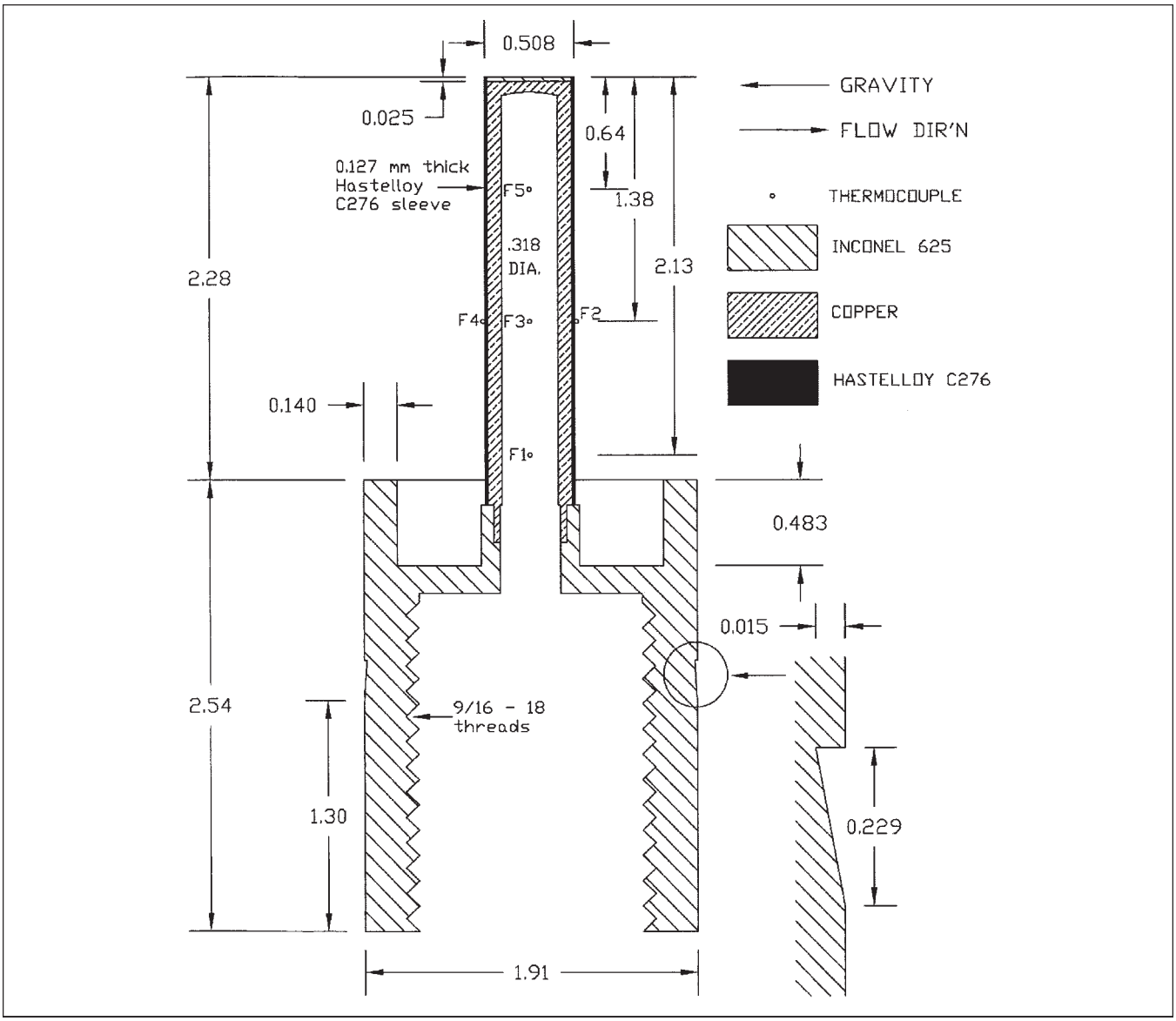

Figure 5. Assembly drawing (to scale) of the hot finger.

Thermocouples are denoted by F1 through F5. All dimensions are in centimeters.

thermocouples measuring the surface temperature profile along the hot finger was ±3.5°C. A small fraction of the heat supplied to the hot finger is conducted through the Inconel 625 base and into the bulk solution over an area where salt is not depositing. Analyses predict that about 90% of the heat supplied to the hot finger drives deposition (Hodes, 1998). The uncertainty in the salt porosity values reported is estimated to be ±15% (Hodes, 1998).

Analysis

The temperature profile along the surface of the hot finger as a function of time was measured during a deposition experiment in which the mass fraction of sodium sulfate in the inlet solution was 4%. Figure 6 shows the results along with the measured bulk solution temperature and estimated SLSI temperature (from Hodes et al., 2003b). All of the thermocouple readings are within the expected uncertainty. Note that the surface temperature of the hot finger reaches about 390°C, a temperature at which sodium sulfate is (pragmatically) insoluble in water at 25 MPa.

The solubility data for Na_2SO_4 and K_2SO_4 in water at 25 MPa are presented in Table 1. Note that the solubility temperature of K_2SO_4 at a mass fraction of 6% was measured in both run F and run I to check repeatability and the measured solubility temperatures agree to within 0.3°C.

The deposition rate data are reported in Table 2. Volumetric flow rates of solution (10 mL/min at 20°C and 25 MPa) were converted to mass flow rates by extrapolating from available data for the aqueous salt solutions (Hodes, 1998). [The addition of sodium sulfate or potassium sulfate to pure water increases its density by only a modest amount (<10%).] Two values for the measured bulk temperature of the solution in the cell are reported; that is, $T_{bulk\,i}$ is that at the beginning of a run and $T_{bulk\,f}$ is that 2 to 3 min before the end of a run. During the

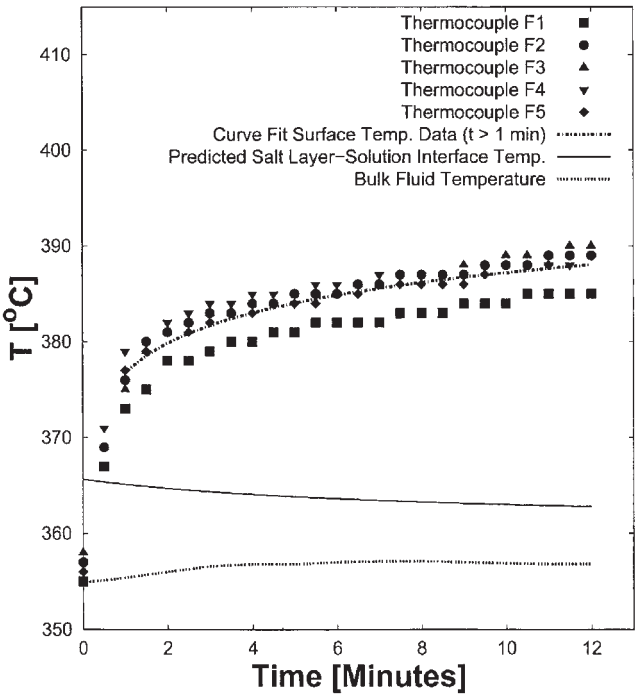

Figure 6. Measured temperatures along the hot finger surface, measured bulk solution temperature, and estimated SLSI temperature profile.

C_{in} = 4%ω Na_2SO_4, pressure = 25 MPa, P = 10.6 W, $\dot{m}$ = 10.47 g/min.

majority of the time elapsed during each run, the bulk solution temperature is closer to $T_{bulk\,f}$ than to $T_{bulk\,i}$. The bulk temperature of the solution in the cell increased by up to about 3°C during each run.

The porosity of the salt layer formed on the hot finger (ϕ) is defined as the void volume divided by the total volume of the layer including voids. The apparent volume of salt (inclusive of voids) was estimated from photographs similar to those shown in Figures 2 and 3 and the true volume occupied by the salt was calculated from the mass of salt deposited by using values of 2680 and 2662 kg/m^3 for the densities of solid Na_2SO_4 and K_2SO_4, respectively (Lide, 1993). Porosity could be calculated only for the selected runs for which the deposited salt was photographed.

The salt concentration averaged over time in the system effluent, denoted by $\bar{\omega}_{eff}$, was calculated according to a mass balance and is reported in Table 2. The difference between the mass fraction of salt in the inlet and effluent streams did not exceed 0.02. Therefore, deposition did not decrease the total mass flow rate of solution through the system by more than about 2%. The measured pressure drop across the system was less than 0.1 MPa in all runs. Finally, it is noted that after several runs, X-ray diffraction (XRD) analyses were performed on the deposited salt and showed that it was exclusively sodium sulfate or potassium sulfate.

Discussion

Solubility measurements

A number of other investigators have measured the solubility of sodium sulfate in water at a pressure of 25 MPa, as shown in Figure 7. [The data from Ravich and Borovaya (1964) and Shvedov and Tremaine (1997) were interpolated from those spanning a range of pressures around 25 MPa.] The solubility temperatures measured in the six independent studies are consistent to within 7°C or better for a given concentration of sodium sulfate. Ravich and Borovaya (1964) obtained their data by measuring pressure changes in a rocking autoclave. Armellini (1993) and, subsequently, DiPippo (1997) obtained their data in an optically accessible flow cell by detecting precipitation by visual observation or light extinction. Finally, Shvedov and Tremaine (1997) and Rogak and Teshima (1999) precipitated all salt beyond the solubility temperature in isothermal and isobaric tubular reactors and measured the salt concentration in the effluent. Rogak and Teshima (1999) also measured the solubility temperature of sodium sulfate down to salt concentrations as low as 0.000042%ω and found that solubility decreases precipitously near 385°C, the temperature at which the compressibility of pure water is a maximum at 25 MPa. The consistent solubility data achieved by different measurement techniques suggest that equilibrium solubility temperatures were measured. Had any of the methods been conducive to metastability, the solubility temperature for a given salt concentration would have been higher. It is noted that the particular curve fit to the solubility data used to select the operating conditions in the deposition experiments and subsequently analyze the results was consistent with the solubility measurements in this study. This is important because the deposition driving force is a strong function of the solubility curve.

Benrath et al. (1937) measured the solubility of potassium sulfate in water at temperatures up to 357°C, but other relevant data were not found. Benrath et al. (1937) acquired solubility data by visually observing an aqueous potassium sulfate solution inside an illuminated sealed glass tube. The highest temperature for which all the salt remained dissolved was the solubility temperature. Benrath et al. (1937) did not measure pressure and their relevant solubility data are shown in Figure 8 along with those from this study. Solubility temperatures measured in this study exceeded those measured by Benrath et al. (1937) by about 15°C. However, the solubility data from the present study were obtained at a higher pressure (25 MPa) than those of Benrath et al. (1937). To be sure, both liquid and vapor phases were present in the Benrath et al. (1937) experiments; therefore, the pressure in their cell was below the critical pressure of pure water (22.1 MPa). The static dielectric constant of water increases with density; therefore, aqueous salt solutions at higher pressures (and thus densities) are expected to have higher solubility temperatures for the same salt concentration.

Table 1. Solubility Data for Na_2SO_4 and K_2SO_4 in Water at 25 MPa

Run	Salt	%ω	T_s (°C)
L	Na_2SO_4	10	342.5
O	Na_2SO_4	3	362.8
F	K_2SO_4	6	375.9
H	K_2SO_4	4	379.1
I	K_2SO_4	6	375.6
J	K_2SO_4	2	382.2
K	K_2SO_3	8	373.5

Table 2. Experimental Deposition Rate Data and Associated Parameters

Run	Salt	$\dot{m}_{soln}$ (g/min)	ω_{inlet} (%)	Time (min)	$T_{bulk\ i}$ (°C)	$T_{bulk\ f}$ (°C)	M_{dep} (g)	$\bar{\omega}_{eff}$ (%ω)	ϕ (%)
18	Na_2SO_4	10.47	4	5.92	355.0	357.2	0.45	3.27	82
6	Na_2SO_4	10.47	4	6.22	355.0	355.5	0.51	3.22	—
8	Na_2SO_4	10.47	4	9.1	355.0	357.6	0.58	3.39	—
17	Na_2SO_4	10.47	4	9.33	355.0	357.3	0.62	3.37	81
19	Na_2SO_4	10.47	4	11.92	355.0	357.6	0.88	3.29	71
9	Na_2SO_4	10.47	4	11.95	355.0	357.5	0.92	3.26	—
15	Na_2SO_4	10.28	2	9.27	363.3	365.8	0.37	1.61	—
14	Na_2SO_4	10.66	6	9.08	347.7	349.9	1.39	4.56	71
13	Na_2SO_4	10.85	8	8.85	340.8	343.9	1.77	6.16	76
U	Na_2SO_4	10.85	8	9.00	340.8	343.1	1.55	6.41	63.2
V	Na_2SO_4	10.66	6	9.03	347.7	350.2	1.06	4.90	62.6
W	Na_2SO_4	10.66	6	9.28	347.7	350.0	1.13	4.86	60.2
Q	K_2SO_4	10.39	4	8.83	371.9	373.6	0.97	2.94	68.4
R	K_2SO_4	10.72	8	8.82	366.1	368.1	1.92	5.97	66.5
S	K_2SO_4	10.56	6	9.02	369.0	371.1	1.37	4.56	67.2
T	K_2SO_4	10.23	2	8.95	374.7	376.7	0.27	1.71	—
Y	K_2SO_4	10.72	8	8.98	366.2	369.0	1.73	6.20	66.0
Z	K_2SO_4	10.39	4	9.60	372.0	373.5	0.91	3.09	67.9

Deposition rate model

A simple model for the rate of salt deposition at the SLSI formed on the hot finger is developed below. It does not account for deposition inside the porous salt layer (PSL) formed on the hot finger and thus predicts only the fraction of the total deposition rate attributable to deposition at the SLSI. The qualitative results produced by this simple model are general, however, and apply to the conditions investigated. The intent is to be quantitatively approximate, but to elucidate the physics of the processes that control the deposition rate.

A linear relationship between salt solubility and temperature is assumed and the simplest form of the analogy between heat and mass transfer is applied. The depletion of salt in the bulk solution because of deposition is not addressed and buoyancy forces induced by (salt) concentration gradients are neglected. Finally, the transient deposition rate is not computed; that is, the mass of salt deposited during each run is calculated from the initial deposition rate. All of the foregoing assumptions have been relaxed in the more rigorous model by Hodes et al. (2003). It is further assumed that all salt diffusing to the SLSI (permanently) sticks to it. Finally, heat and mass transfer coefficients are set equal to their mean values for laminar natural convection along a vertical flat plate of height $\pi D_{HF}/2$.

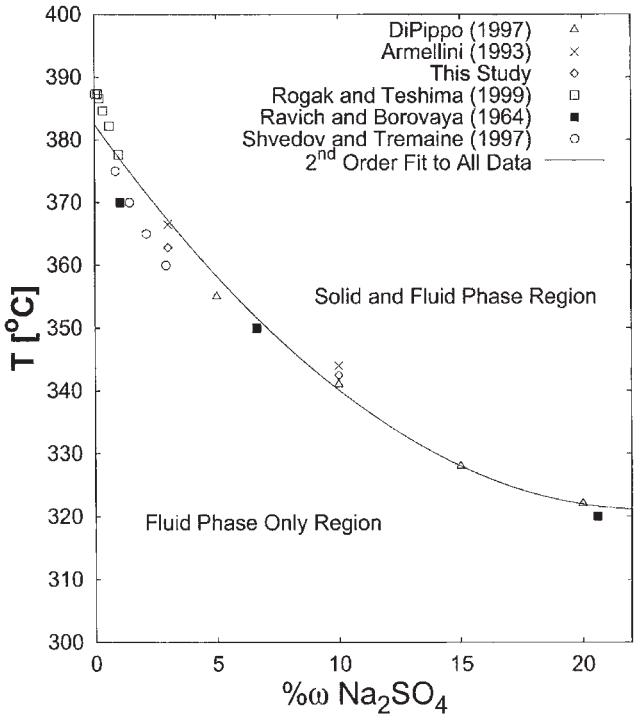

Figure 7. Temperature–composition diagram for the Na_2SO_4–H_2O system at 25 MPa.

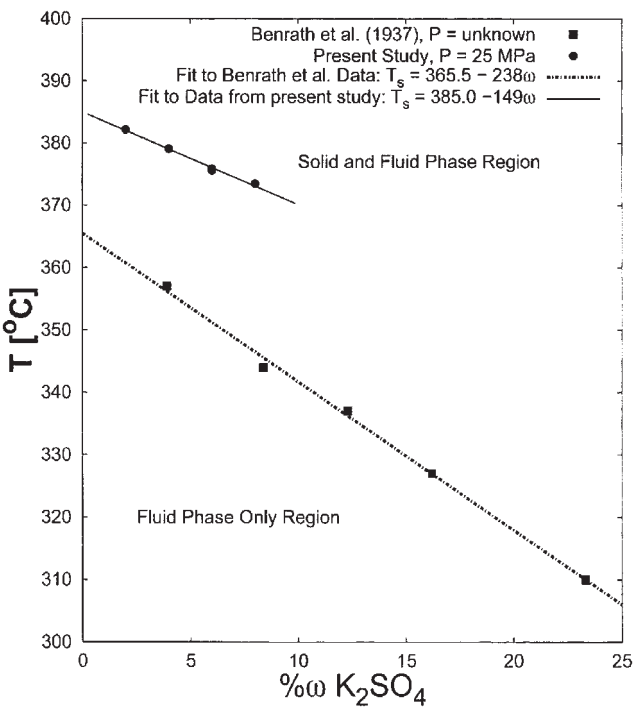

Figure 8. Potassium sulfate in water solubility data from this study and from Benrath et al. (1937).

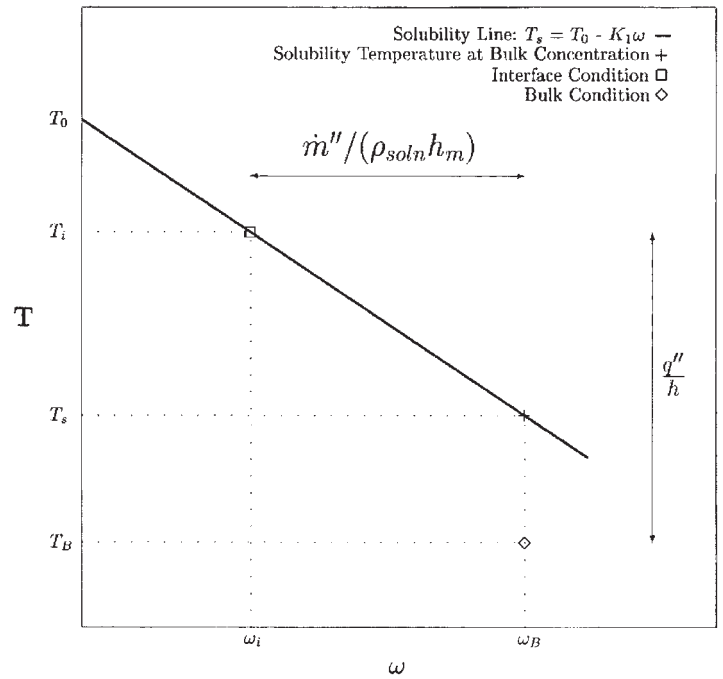

Figure 9. Temperatures, concentrations, and illustrations of principles relevant to the relationship between transport coefficients and deposition rate at the SLSI.

Contrary to what one might expect, a reduction in transport coefficients may increase, decrease, or not affect the deposition rate at the SLSI. Temperatures, concentrations, and graphic illustrations of principles required to derive the relationship between the transport coefficients and the deposition rate are shown in Figure 9. The solubility relationship is assumed to be $T_s = T_0 - K_1\omega$, where T_s and T_0 are the solubility temperatures corresponding to the bulk salt concentration and to (pragmatically) zero salt concentration, respectively. The heat and mass transfer coefficients relate the heat flux (q'') and mass flux, respectively, at the SLSI to their driving forces, that is

$$T_i = T_B + \frac{q''}{h} \tag{1}$$

$$\dot{m}'' = h_m\rho_{soln}(\omega_B - \omega_i) \tag{2}$$

When the SLSI temperature (T_i) is below that corresponding to zero salt solubility and above the solubility temperature corresponding to the concentration of salt in the bulk solution, the slope of the solubility line may be used to express the driving force for deposition at the SLSI ($\omega_B - \omega_i$) in terms of the temperature difference ($T_i - T_s$) as

$$\omega_B - \omega_i = (T_i - T_s)/K_1 \qquad \text{for } T_s \le T_i \le T_0 \tag{3}$$

It follows that the mass flux of salt to the SLSI when $T_s \le T_i \le T_0$ is

$$\dot{m}'' = \left[\frac{h_m}{h}\,q'' - h_m(T_s - T_B)\right]\frac{\rho_{soln}}{K_1} \qquad \text{for } T_s \le T_i \le T_0 \tag{4}$$

For sufficiently weak transport, the SLSI temperature is greater than or equal to the temperature corresponding to zero salt solubility and the mass flux of salt to the SLSI is simply

$$\dot{m}'' = h_m\rho_{soln}\omega_B \qquad \text{for } T_i \ge T_0 \tag{5}$$

Conversely, for sufficiently strong transport, the SLSI temperature is less than or equal to the solubility temperature corresponding to the concentration of salt in the bulk solution and the deposition rate equals zero.

For both natural and forced convective transport, the Nusselt and Sherwood numbers are generally similar, if not identical, functions of the same set of dimensionless groups, with the exception that the Nusselt number is functionally dependent on the Prandtl number, whereas the Sherwood number is functionally dependent on the Schmidt number. Moreover, for the majority of convection problems the Nusselt number scales as the Prandtl number to some power n and the Sherwood number scales as the Schmidt number to the same power n. Thus, generally

$$\frac{\mathrm{Nu}}{\mathrm{Sh}} \cong \frac{1}{\mathrm{Le}^n} \tag{6}$$

Equation 6 is a form of the analogy between heat and mass transfer. It applies rigorously to natural convection boundary layer flows only when the Lewis number equals unity, but suffices for the simple transport analysis given here. From the definitions of the Nusselt and Sherwood numbers, the analogy between heat and mass transfer (Eq. 6) becomes

$$\frac{h}{h_m} = \rho_{soln} c_p \, \mathrm{Le}^{1-n} \tag{7}$$

where n is about 1/3. Combining Eq. 4 with the analogy between heat and mass transfer, it follows that

$$\dot{m}'' = \rho_{soln}\left[\frac{q''}{\rho_{soln} c_p \, \mathrm{Le}^{1-n}} - h_m(T_s - T_B)\right]\Big/ K_1 \qquad \text{for } T_s \le T_i \le T_0 \tag{8}$$

When the heat flux at the SLSI, relevant solution properties and bulk solution temperature are constant and $T_s \le T_i \le T_0$, the mass flux of salt deposited at the SLSI *increases* linearly with a *decreasing* mass-transfer coefficient. This is because a reduction in the mass-transfer coefficient is accompanied by an increase in the mass-transfer driving force and the net effect is an increase in the deposition rate at the SLSI.

An absolute maximum in the mass flux of salt to the SLSI as a function of the mass-transfer coefficient occurs at the value of the mass transfer coefficient for which the SLSI temperature equals that corresponding to zero salt solubility. The mass transfer coefficient at this condition is subsequently referred to as the critical mass-transfer coefficient, which may be determined from Eq. 1 and the analogy between heat and mass transfer. It is given by Eq. 9 and the corresponding mass flux is given by Eq. 10. Further reductions in the mass-transfer coefficient do not change the mass transfer driving force and thus decrease the mass flux to the SLSI.

$$h_{m,c} = \frac{q''}{\rho_{soln} c_p \, \mathrm{Le}^{1-n}(T_0 - T_B)} \tag{9}$$

$$\dot{m}''\big|_{max} = h_{m,c}\rho_{soln}\omega_B \tag{10}$$

Finally, the condition for $T_i \le T_s$ (that is, zero deposition) may also be expressed in terms of the mass-transfer coefficient. From Eq. 1 and the analogy between heat and mass transfer it follows that $T_i \le T_s$ if $h_m \ge q''/[\rho_{soln} c_p \, \mathrm{Le}^{1-n}(T_s - T_B)]$.

The relationship between the mass flux at the SLSI and the mass-transfer coefficient is illustrated in Figure 10 for an arbitrary set of conditions. The mass flux of salt to the SLSI is nondimensionalized by its maximum value and the mass transfer coefficient by the critical mass-transfer coefficient. The dimensionless mass flux increases linearly with the dimensionless mass-transfer coefficient until the critical mass-transfer coefficient is reached. Moreover, the derivative of the dimensionless mass flux with respect to the dimensionless mass transfer coefficient equals one when $h_m \le h_{m,c}$. For $h_m > h_{m,c}$, dimensionless mass flux decreases linearly with dimensionless mass-transfer coefficient until deposition ceases for $h_m \ge q''/[\rho_{soln} c_p \, \mathrm{Le}^{1-n}(T_s - T_B)]$.

The simple mass-transfer model was applied to the conditions in the deposition experiments, except when the mass fraction of sodium sulfate in the inlet stream was 8% because the phase boundary for the Na_2SO_4–H_2O system becomes nonlinear at Na_2SO_4 mass fractions above 6%. Transport coefficients were calculated from a Nusselt number expression ($Nu_x = 0.4010 Gr_x^{1/4}$) from Gebhart et al. (1988) for natural convection heat transfer along a vertical flat plate when the Prandtl number equals unity. (At the conditions investigated in the deposition experiments, the Prandtl number of pure water is near unity.) The aqueous salt solutions were approximated as pure water and relevant thermophysical properties were obtained from the NBS Steam Tables (Gallagher, 1985). The duration of each deposition experiment was approximately 6, 9, or 12 min and the mass of salt deposited, M_{exp}, was normalized to 6.0, 9.0, or 12.0 min by assuming a constant deposition rate. The bulk temperature characterizing the end of the runs at each condition was used in the calculations. The modeling results and experimental data are presented in Table 3. The ratio $h_m/h_{m,c}$ was greater than unity for all the runs except one (Run 15) in which it was almost unity. Therefore, the analysis predicts that a reduction in the mass-transfer coefficient leads to an increase in the deposition rate at the SLSI except in Run 15. The ratio $h_m/h_{m,c}$ is an increasing function of the salt concentration in the inlet stream according to Table 3.

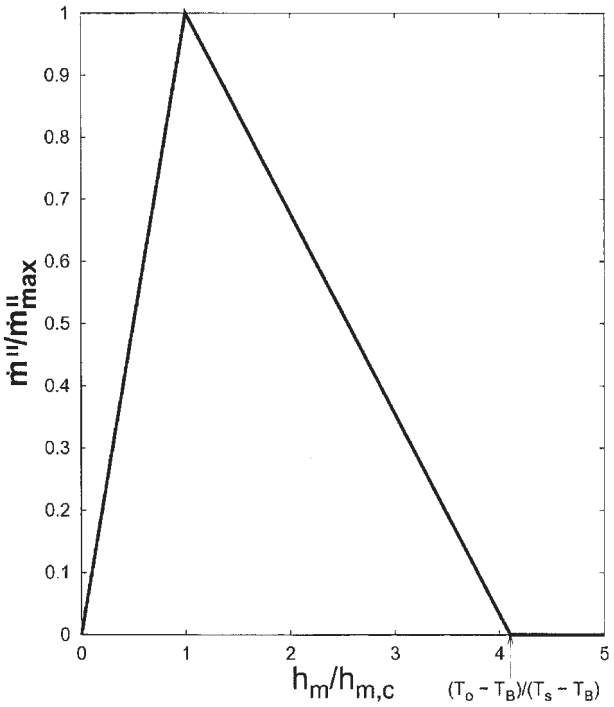

Figure 10. Relationship between the dimensionless mass flux and dimensionless mass transfer coefficient at the SLSI.

The ratio of the calculated mass of salt deposited on the hot finger to that measured, M_{theory}/M_{exp}, ranges from 1.16 to 4.45. However, the model assumes that the salt layer is impervious and that deposition therefore occurs exclusively at the SLSI. In fact, the salt layer is quite porous and deposition occurs within the matrix except when the fluid in the pores is pure water ($h_m/h_{m,c} < 1$) under which conditions deposition in the pores is impossible. This is presumably the reason for the better agreement between theory and experiment when $h_m/h_{m,c} \cong 1$ than when it is significantly >1. Note that, for the sodium sulfate and potassium sulfate results, M_{exp}/M_{theory} is closest to unity when $h_m/h_{m,c}$ is closest to 1.0, as expected. Also, the trends in the discrepancies between the model and data are

Table 3. Application of the Deposition Rate Model to the Conditions Investigated Experimentally

Run(s)	Salt	$\%\omega$	Time (min)	$T_{bulk\,f}$ (°C)	$h_m/h_{m,c}$	M_{theory} (g)	M_{exp} (g)	M_{exp}/M_{theory}
15	Na_2SO_4	2	9.0	365.8	0.98	0.31	0.36	1.16
18, 6	Na_2SO_4	4	6.0	357.5	1.80	0.25	0.46, 0.49	1.84, 1.96
8, 17	Na_2SO_4	4	9.0	357.5	1.80	0.37	0.57, 0.60	1.54, 1.62
19, 9	Na_2SO_4	4	12.0	357.5	1.80	0.49	0.89, 0.92	1.82, 1.88
14, V, W	Na_2SO_4	6	12.0	350.0	2.51	0.43	1.38, 1.06, 1.10	3.21, 2.47, 2.56
T	K_2SO_4	2	9.0	376.7	1.02	0.14	0.27	1.93
Q, Z	K_2SO_4	4	9.0	373.6	1.33	0.23	0.99, 0.85	4.30, 3.70
S	K_2SO_4	6	9.0	371.1	1.57	0.33	1.37	4.15
R, Y	K_2SO_4	8	9.0	368.5	1.81	0.44	1.96, 1.73	4.45, 3.93

consistent with deposition inside the porous salt layer accounting for a larger fraction of the mass of salt deposited as $h_m/h_{m,c}$ increases beyond 1.0. For the sodium sulfate deposition data, M_{exp}/M_{theory} monotonically increases with salt concentration (that is, with $h_m/h_{m,c}$) presumably because deposition in the porous salt layer becomes more important. For the potassium sulfate case, the deposition rate approximately doubles when salt concentration increases from 2 to 4% mass fraction (that is, as $h_m/h_{m,c}$ increases from 1.02 to 1.33), but remains approximately at a constant value as $h_m/h_{m,c}$ is further increased. Finally, it is noted that the more rigorous model for the deposition rate at the SLSI by Hodes et al. (2003b) is consistent with the present one with respect to the importance of deposition within the PSL. To be sure, when compared to the experimental data, both models indicate that the deposition rate in the PSL is comparable to that at the SLSI at sufficiently high salt concentrations.

Conclusions

A method to measure the solubility of salts in water at the elevated temperatures and pressures typical of SCWO has been developed. Measured solubility temperatures in aqueous, sodium sulfate solutions compare well with data in the literature, thereby validating the method. The solubility temperature of potassium sulfate in water at a pressure of 25 MPa corresponding to salt concentrations of up to 8% mass fraction was measured for the first time. Transient deposition rate data from near-supercritical, aqueous, sodium sulfate and potassium sulfate solutions to a hot finger were collected. Salt mass fractions in the bulk solution around the hot finger ranged from 2 to 8%. The salt deposition rate was on the order of 1 g/min. Natural convection was the dominant mechanism of transport at all experimental conditions. At the conditions investigated in the deposition experiments, a simple model using the analogy between heat and mass transfer was developed to predict the deposition rate at the salt layer–solution interface and elucidate the relationship between transport coefficients and deposition rate. The discrepancy between the model prediction and the experimental data is postulated to be largely attributable to deposition within the porous salt layer, which is not accounted for in the model, and the trends in the discrepancies between model and data are consistent with this hypothesis.

Acknowledgments

The authors thank Maria Aquino-Class of the Process Measurements Division at NIST for performing the (ex situ) X-ray diffraction analyses of salt deposited on the hot finger.

Notation

c_p = heat capacity at constant pressure, J/(kg · K)
D = diameter, m
g = acceleration attributed to gravity, m/s^2
Gr = Grashof number
h = (mean) heat transfer coefficient, W/(m^2 · K)
h_m = (mean) mass transfer coefficient, m/s
$h_{m,c}$ = critical mass transfer coefficient, m/s
Le = Lewis number
$\dot{m}_{soln}$ = mass flow rate of solution, kg/s
$\dot{m}''$ = mass flux of salt to SLSI, kg/(m^2 · s)
$M_{deposited}$ = mass of salt deposited for entire run, g or kg
$\overline{\mathrm{Nu}}$ = mean Nusselt number
q'' = heat flux at SLSI, W/m^2
$\overline{\mathrm{Sh}}$ = mean Sherwood number
t = time, s or min
T = temperature, °C

Greek letters

ρ_{soln} = density of aqueous salt solution, kg/m^3
ϕ = porosity
ω = mass fraction of salt in solution

Subscripts

B = bulk condition
bulk i = initial bulk condition
bulk f = bulk condition 2–3 min before end of run
eff = effluent
HF = hot finger
in = inlet
0 = temperature corresponding to zero salt solubility
s = solubility
SLSI or i = salt layer–solution interface

Literature Cited

American Society for Testing and Materials (ASTM), *1992 Annual Book of ASTM Standards,* Vol. 14.03, Philadelphia, PA (1992).
Armellini, F. J., "Phase Equilibria and Precipitation Phenomena of Sodium Chloride and Sodium Sulfate in Sub- and Supercritical Water," PhD Thesis, Massachusetts Institute of Technology, Cambridge, MA (1993).
Benrath, V. A., F. Gjedebo, B. Schiffers, and H. Wunderlich, "Über die Löslichkeit von Salzen und Salzgemischen in Wasser bei Temperaturen oberhalb von 100°C," *Z. Anorg. Allg. Chem.,* **231**, 285 (1937).
DiPippo, M. M., "Phase Behavior of Inorganic Salts in Sub- and Supercritical Water," PhD Thesis, Massachusetts Institute of Technology, Cambridge, MA (1997).
Gallagher, J. S., and L. Haar, *NBS Standard Reference Database 10 Steam Tables,* National Bureau of Standards, Washington, DC (1985).
Gebhart, B., Y. Jaluria, R. L. Mahajan, and B. Sammakia, *Buoyancy-Induced Flow and Transport,* Hemisphere Publishing, New York (1988).
Hodes, M., "Measurements and Modeling of Deposition Rates from Near-Supercritical, Aqueous, Sodium Sulfate and Potassium Sulfate Solutions

to a Heated Cylinder," PhD Thesis, Massachusetts Institute of Technology, Cambridge, MA (1998).
Hodes, M., P. A. Marrone, G. T. Hong, K. A. Smith, and J. W. Tester, "Salt Precipitation and Scale Control in Supercritical Water Oxidation—Part A: Fundamentals and Research," *J. Supercrit. Fluids,* **29,** 265 (2004).
Hodes, M., K. A. Smith, and P. Griffith, "A Natural Convection Model for the Rate of Salt Deposition from Near-Supercritical Aqueous Solutions," *J. Heat Transfer,* **125**(6), 1027 (2003).
Hurst, W. S., M. Hodes, W. J. Bowers, Jr., V. E. Bean, J. E. Maslar, P. Griffith, and K. A. Smith, "Optical Flow Cell and Apparatus for Solubility, Salt Deposition and Raman Spectrographic Studies in Aqueous Solutions near the Water Critical Point," *J. Supercrit. Fluids,* **22**, 157 (2002).
Lide, D. R., ed., *CRC Handbook of Chemistry and Physics,* 74th Edition, CRC Press, Boca Raton, FL (1993).
Marrone, P. A., M. Hodes, K. A. Smith, and J. W. Tester, "Salt Precipitation and Scale Control in Supercritical Water Oxidation—Part A: Commercial/Full-Scale Applications," *J. Supercrit. Fluids,* **29,** 289 (2004).
Ravich, M. I., and V. Y. Borovaya, "Phase Equilibrium in Water–Salt Systems at High Pressures and Temperatures," *Russ. J. Inorg. Chem.,* **9**, 520 (1964).
Rogak, S. N., and P. Teshima, "Deposition of Sodium Sulfate in a Heated Flow of Supercritical Water," *AIChe J.,* **45**(2), 240 (1999).
Shaw, R. W., T. B. Brill, A. A. Clifford, C. A. Eckert, and E. U. Franck, "Supercritical Water: A Medium for Chemistry," *Chem. Eng. News,* **26**(Dec.), 26 (1991).
Shvedov, D., and P. R. Tremaine, "The Solubility of Aqueous Sodium Sulphate and the Reduction of Sulphate by Magnetite Under Near-Critical Conditions," Proc. of the 5th Int. Symp. on Hydrothermal Reactions, Gatlinburg, TN, p. 239 (1997).
Smith, K. A., M. Hodes, and P. Griffith, "On the Potential for Homogeneous Nucleation of Salt from Aqueous Solution in a Natural Convection Boundary Layer," *J. Heat Transfer,* **124**(5), 930 (2002).
Tester, J. W., H. R. Holgate, F. J. Armellini, P. A. Webley, W. R. Killilea, G. T. Hong, and H. E. Barner, "Supercritical Water Oxidation Technology: Process Development and Fundamental Research," *Emerging Technologies in Hazardous Waste Management III,* ACS Symposium Series 518, W. D. Tedder and F. G. Pohland, eds., American Chemical Society, Washington, DC, p. 35 (1993).

Manuscript received May 13, 2003, revision received Nov. 2, 2003, and final revision received Feb. 13, 2004.